Passivity-based control design for a grid-connected hybrid generation system integrated with the energy management strategy

M. Patrone[a,*], D. Feroldi[a,b]

[a] *French-Argentine International Centre for Information and System Sciences (CIFASIS-CONICET-UNR), 27 de Febrero 210 bis, S2000EZP Rosario, Argentina.*
[b] *Department of Computer Sciences, FCEIA-UNR, Rosario, Argentina.*

Abstract

Hybrid generation systems produce electric energy from a wide variety of energy sources, including renewable sources. A hybrid system based on renewable sources usually consists of two or more renewable energy sources with the possibility of including storage units so as to enhance the reliability of the system. The hybrid system requires an energy strategy that determines the operation point of each element of the system depending on multiple variables and subjected to the constraints inherent in this kind of systems. In addition, the system needs controllers to command each of these elements in order to reach the operation point established by the energy strategy. Here, we propose a control design via passivity-based control integrated with an energy management strategy for a hybrid generation system based on solar energy and coupled with the grid. The performance of the control methodology is extensively assessed through computer simulation using a

*Corresponding author
Email addresses: patrone@cifasis-conicet.gov.ar (M. Patrone), feroldi@cifasis-conicet.gov.ar (D. Feroldi)

Preprint submitted to Journal of Process Control *October 31, 2017*

comprehensive nonlinear model of the plant. The results show that the controlled system accomplishes the control tasks with good responses, working under very different atmospheric conditions and required load power.
Keywords: Hybrid generation system, Passivity-based control, Euler-Lagrange equations, Solar energy

1. Introduction

Energy consumption has considerably increased in the last few decades since the progression of socio-economic activities is closely connected with the access to electric energy. But satisfying this increasing consumption with fossil fuels is no longer possible due to their high level of emissions that contribute to global warming with devastating consequences for the environment. In this context, the use of renewable energies can overcome the growing energy demand with a minor impact on the environment [1].

Renewable energy sources are desirable for electrical power generation because they have many advantages including sustainability, low pollution and economic benefits. Due to the intermittent nature of many renewable resources, a combination of more than one source may be helpful towards obtaining a more reliable system, constituting a hybrid generation system (HGS). Also, a hybrid system can be complemented with a storage system to overcome periods of scarce generation reducing even more the probability of energy supply shortage. A hybrid system composed of renewable sources and storage elements is defined as stand-alone (SA) system, which is suitable for remote locations where the grid cannot penetrate and there is no other energy source. However, if the grid is accessible, the hybrid system could be coupled to the electricity grid conforming a grid-connected (GC) system. Although both SA and GC present many advantages, the choice of GC or SA system may depend on a number of factors but primarily on electricity accessibility [2].

In general, each element of the HGS is linked to a DC or AC bus through power converters. A control system is implemented to command each power converter, and therefore the behaviour of the HGS. This control system could be divided in two levels with specific control tasks, depending on its hierarchical position. The low level is composed of the controllers of the power converters which command the electronic switches to satisfy specific current or voltage references. These references are established by a supervisory control or energy manager in order to satisfy the power demand of the load, subjected to the constraints of the system. Different approaches for addressing the control system are found in the literature. For example, in [3] a stand-alone HGS is presented where the control law is designed through the combination of passivity and sliding mode techniques. Another example of SA applications could be found in [4] but there a PI controller is considered. A GC application could be found in [5] where they have also used PI controllers. In this paper, we are particular interested in passivity-based control (PBC) methods to command the converters.

PBC is a controller design technique based on physical principles, namely, the energy and damping features of the system. Using physical principles, the dynamic behaviour of a system could be described by means of its energy. Furthermore, a complex system may also be decomposed into simpler subsystems that add up their energies to determine the full behaviour of the system. Similarly, the controller could be understood in terms of energy as another dynamical system interconnected with the plant to achieve a desirable behaviour in closed loop. Then, the control problem can be reformulated as designing a controller that shapes the energy function of the system so that the overall energy function takes the desired form. PBC is based on this energy-shaping approach. A complete report on PBC is presented in [6] and [7].

The fact that PBC is based on the physical principles of the system explains its success to control physical systems with non-negligible nonlinearities. For example, this method has been primarily used to control AC drives [8, 9] and mechanical systems [10]. However, this methodology has been extended to address the control problem of the HGS. For instance, Ayad et al. [11] have controlled a hybrid system composed of ultracapacitors and fuel cell. A PBC strategy has been used to control an electric vehicle with supercapacitors and batteries as storage elements [12]. Also, Tofighi and Kalantar [13] used PBC to control a hybrid power source comprised of a photovoltaic (PV) system and Li-ion batteries and PBC has also been used to control systems in power electronics [14].

In this paper, a grid-connected hybrid generation system composed of PV arrays and two different types of storage elements is addressed. The PV system is the main power of energy and the storage system enhances the reliability of the overall system. The main priority is to satisfy the load demand using the grid as an ancillary energy source with the possibility of selling any surplus generation. The HGS is described mathematically by means of Euler-Lagrange equations and the control laws are achieved by

PBC. The main contribution of this article is the integration of the controllers designed via passivity-based control with the energy management strategy (EMS) to fulfil the mentioned objectives.

The paper is organized as follows. In Section 2, we give a detailed description of the hybrid generation system. Section 3 presents the Euler-Lagrange model of the system. In Section 4, we design the controller following the Standard PBC procedure. Section 5 presents the energy management strategy using a finite-state machine approach. In Section 6, the results of several simulations are presented and discussed. Finally, conclusions are stated in Section 7.

2. System description

This section presents the hybrid generation system (HGS) and also the modelling of its different parts. Figure 1 depicts the structure of the system under study in this work. The HGS is comprised of battery and supercapacitor banks, DC and AC loads, and PV arrays. Also, the system is coupled with an electrical network modelled by an ideal AC voltage source. The main objective of the system is to supply the required power to the loads exploiting the renewable resources and avoiding, if it is possible, power flow from the grid.

2.1. Solar energy system

The electric behaviour of a photovoltaic cell could be modelled by a non-linear current source connected in series with the intrinsic cell resistance. A PV array is a group of individual cells connected in series and parallel to fulfil

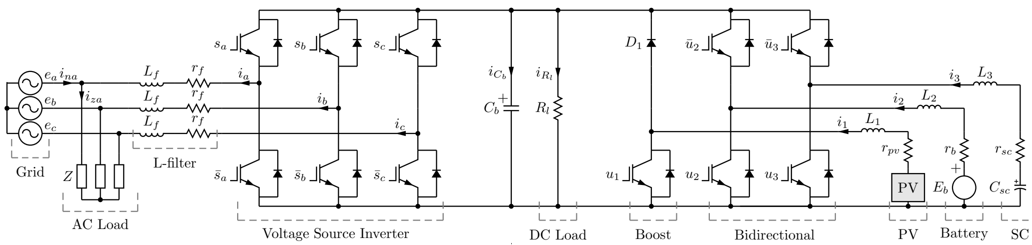

Figure 1: Hybrid system structure.

the grid voltage and current requirements. Therefore, the current provided by a PV array is defined implicitly by the following equation [15]:

$$i_{pv}(t) = n_p^{pv}\left[i_{ph}(t) - i_{rs}(t)\left(exp\left(\frac{q(v_{pv}(t) + i_{pv}(t)r_s)}{n_s^{pv}A_cKT(t)}\right) - 1\right)\right], \tag{1}$$

where n_s^{pv} and n_p^{pv} indicate de number of cells connected in series and parallel, respectively. v_{pv} is the voltage level on the PV panel array terminals, A_c is the cell deviation from the ideal p-n junction characteristic, i_{rs} is the cell reverse saturation current, i_{ph} is the generated current under a given insolation, q is the electron charge, K is the Boltzman constant, r_s is the intrinsic cell resistance and T is the cell temperature. i_{ph} and i_{rs} depend on the insolation and cell temperature according to the following expressions:

$$i_{rs}(t) = I_{or}\left(\frac{T(t)}{T_{ref}}\right)^3 exp\left(\frac{qE_{go}(1/T_r - 1/T(t))}{KT(t)}\right), \tag{2}$$

$$i_{ph}(t) = (I_{sc} + K_l(T(t) - T_r))\lambda(t)/100, \tag{3}$$

where E_{go} is the band-gap energy of the semiconductor used in the cell, I_{or} is the reverse saturation current at the reference temperature T_{ref}, I_{sc} is the short-circuit cell current at the reference temperature and insolation, λ is the insolation in mW/cm^2, and K_l is the short-circuit current temperature coefficient. The values of these constants are given in Table 1.

The instantaneous energy generated by a photovoltaic cell depends on the insolation and the cell temperature. Thus, in order to maximize the power extraction under varying atmospheric conditions there are several techniques which find the v_{pv} values that locate the operating point of the PV cell at the Maximum Power Point (MPP) [16].

2.2. Energy storage system

In this work, we decided to use lead-acid batteries as the energy storage elements with high specific energy. Each battery is modelled as a controlled voltage source (E_b) in series with an internal resistance (r_b) [17]. The lead-acid batteries could be described by the following equations:

$$E_b = E_0 - K_b \frac{Q}{Q - it} \cdot (it + p_1 \cdot i_b^*) + Exp, \tag{4}$$

$$\dot{Exp} = B|i_b|(-Exp + A \cdot p_2), \tag{5}$$

$$p_1 = \begin{cases} 1 & \text{discharge mode,} \\ \frac{Q-it}{it-0.1Q} & \text{charge mode,} \end{cases} \tag{6}$$

$$p_2 = \begin{cases} 0 & \text{discharge mode,} \\ 1 & \text{charge mode,} \end{cases} \tag{7}$$

E_0 : Battery constant voltage (V),

K_b : Polarisation constant (V Ah^{-1}),

Q : Battery capacity (Ah),

$it = \int \frac{i_b}{3600}\, dt$: Actual battery charge (Ah),

i_b^* : Filtered current (A),

Exp : Exponential zone voltage (V),

A : Exponential zone amplitude (V),

B : Exponential zone time constant inverse (Ah^{-1}),

t : Time (s).

The SOC_b is the available energy capacity expressed as a percentage of its rated energy capacity and it could be expressed as:

$$SOC_b = 1 - it/Q. \tag{8}$$

The energy storage system is completed with a supercapacitor bank. These elements possess a high specific power; hence, it is sized for peak power requirements. We model the supercapacitor bank as an ideal capacitor with high capacity (C_{sc}) in series with an internal resistance (r_{sc}). Similarly to the battery bank, the SOC is defined as:

$$SOC_{sc} = q_{sc}/Q_{sc}, \tag{9}$$

where q_{sc} is the supercapacitor charge and $Q_{sc} = V_{sc}^n C_{sc}$ is the total charge capacity. V_{sc}^n is the supercapacitor nominal voltage.

There are constraints that must be considered in order to ensure good performance and useful life:

$$I_x^m \leq i_x \leq I_x^M, \tag{10}$$

$$SOC_x^m \leq SOC_x \leq SOC_x^M, \quad x = b, sc, \tag{11}$$

where the superscript m and M indicate the minimum and maximum value allowed, respectively.

2.3. Loads

A DC load modelled by a resistor (R_l) is connected in parallel with the bus capacitor (C_b). An AC load modelled by a generic impedance (Z) is connected directly to the grid and coupled with the HGS via a three-level IGBT voltage source inverter (VSI).

2.4. Power converters

The amplitude of the voltage of the PV array depends on the insolation and the cell temperature. Therefore, a boost DC/DC converter is utilized to adjust this voltage. In the case of the battery or the supercapacitor bank a bidirectional DC/DC converter is used so as to regulate the power flow in both directions.

3. Euler-Lagrange modelling of the system

In the previous section we briefly described the power converters and other components. In this section, we obtain their Euler-Lagrange descriptions.

The Euler-Lagrange (EL) equations are a set of differential equations that describe the dynamic behaviour of physical systems. They are derived from the variational principle, which is a powerful method to model physical systems in terms of energy quantities. The starting point of the variational approach to modelling is the definition of the energy function in terms of sets of generalized variables. This procedure leads to the introduction of the Lagrangian function.

The Lagrangian function of the system $\mathcal{L}(\dot{q}, q)$ is the difference in the magnetic co-energy of the inductive elements, denoted by $\mathcal{T}(\dot{q}, q)$, and the electric field energy of the capacitive elements, expressed in terms of $\mathcal{V}(q)$. That is,

$$\mathcal{L}(\dot{q}, q) \triangleq \mathcal{T}(\dot{q}, q) - \mathcal{V}(q), \tag{12}$$

where $q \in \mathbb{R}^n$ are the generalized coordinates describing the circuit. In our case, $q = [q_{C_b}, q_L^\top]^\top$, where $q_L = [q_1, q_2, q_3, q_a, q_b, q_c]^\top$. Each element of q_L and $\dot{q}_L$ represents the electric charge and current corresponding to the three boosting inductors and the filter inductors, respectively. q_{C_b} is the electric charge of the DC bus capacitor (C_b). Before presenting the EL equation, it is necessary to represent the switching actions for the six switches of the VSI by bipolar switches functions s_a, s_b and s_c, with the following definition

$$s_k = \begin{cases} 1, & S_k \text{ closed}, \\ -1, & \bar{S}_k \text{ closed}, \end{cases} \quad \text{with } k = a, b, c. \tag{13}$$

Similarly, we define the state of the remaining switches by $u_i = 1$ when it is closed and $u_i = 0$ otherwise, with $i = 1, 2, 3$. Also, we assume that the conducting resistance of any power switch is negligible.

The EL equation for a non-conservative system is described by

$$\frac{d}{dt}\left(\frac{\partial \mathcal{L}}{\partial \dot{q}}(\dot{q}, q)\right) - \frac{\partial \mathcal{L}}{\partial q}(\dot{q}, q) + \frac{\partial \mathcal{D}}{\partial \dot{q}}(\dot{q}) = \mathcal{Q}, \tag{14}$$

where $\mathcal{D}$ is the Rayleigh dissipation function and $\mathcal{Q} \in \mathbb{R}^n$ are the external forces. In view of the system configuration and the definitions made, we present the following EL parameters:

$$\mathcal{T}(\dot{q}) = \frac{1}{2}\dot{q_L}^\top \boldsymbol{L} \dot{q}_L, \tag{15}$$

$$\mathcal{V}(q) = \frac{1}{2C_b} q_{C_b}^2, \tag{16}$$

$$\mathcal{D}(\dot{q}) = \frac{1}{2}\left[\dot{q_L}^\top \boldsymbol{R} \dot{q}_L + R_l(-\dot{q}_{C_b} - \frac{1}{2}s^\top \dot{q}_f + \bar{u}^\top \dot{q}_{123})^2\right], \tag{17}$$

where $\boldsymbol{L} = \mathrm{diag}(L_1, L_2, L_3, L_f, L_f, L_f)$, $\boldsymbol{R} = \mathrm{diag}(r_{pv}, r_b, r_{sc}, r_f, r_f, r_f)$, $q_f = [q_a, q_b, q_c]^\top$, $q_{123} = [q_1, q_2, q_3]^\top$, $s = [s_a, s_b, s_c]^\top$ and $\bar{u} = [\bar{u}_1, \bar{u}_2, \bar{u}_3]^\top$, with $\bar{u}_i = 1 - u_i$, $i = 1, 2, 3$.

For ease of presentation, we define the current through R_l as $i_{R_l} = -\dot{q}_{C_b} - \frac{1}{2}s^\top \dot{q}_f + \bar{u}^\top \dot{q}_{123}$. A direct calculation of (14) with the EL parameters (15)-(17) yields

$$\frac{q_{C_b}}{C_b} + R_l i_{R_l} \frac{\partial i_{R_l}}{\partial \dot{q}_{C_b}}(\dot{q}) = 0, \tag{18}$$

$$\boldsymbol{L}\ddot{q}_L + \boldsymbol{R}\dot{q}_L + R_l i_{R_l} \mathbb{I}_6 \frac{\partial i_{R_l}}{\partial \dot{q}_L}(\dot{q}) = Q_L, \tag{19}$$

where $\frac{\partial i_{R_l}}{\partial \dot{q}_{C_b}}(\dot{q}) = -1$, $\frac{\partial i_{R_l}}{\partial \dot{q}_L}(\dot{q}) = \left[\frac{\partial i_{R_l}}{\partial \dot{q}_1}, \frac{\partial i_{R_l}}{\partial \dot{q}_2}, \frac{\partial i_{R_l}}{\partial \dot{q}_3}, \frac{\partial i_{R_l}}{\partial \dot{q}_a}, \frac{\partial i_{R_l}}{\partial \dot{q}_b}, \frac{\partial i_{R_l}}{\partial \dot{q}_c}\right]^\top$, $Q_L = [E_{pv}, E_b, E_{sc}, -e_n^\top]^\top$ and $e_n = [e_a, e_b, e_c]^\top$ is a vector in which each element represents the line voltage of the ideal AC voltage source. $\mathbb{I}_n$ is the identity matrix of dimension n.

Using the definition of i_{R_l}, replacing (18) in (19) and after some algebraic manipulation we get

$$\dot{q}_{C_b} + \frac{1}{2}s^\top \dot{q}_f + \frac{q_{C_b}}{R_l C_b} - \bar{u}^\top \dot{q}_{123} = 0, \tag{20}$$

$$\boldsymbol{L}\ddot{q}_L + \boldsymbol{R}\dot{q}_L + \frac{q_{C_b}}{C_b} \mathbb{I}_6 \frac{\partial i_{R_l}}{\partial \dot{q}_L}(\dot{q}) = Q_L. \tag{21}$$

Now, we expand (21) with respect to each component in a new set of variables $w = [v_{C_b}, i_L^\top]^\top$, where we have used $i = \dot{q}$ and $v_{C_b} = q_{C_b}/C_b$. Under these considerations, the EL model now has the form

$$C_b \dot{v}_{C_b} + \frac{1}{2}s^\top i_f + v_{C_b} R_l^{-1} - \bar{u}^\top i_{123} = 0, \tag{22}$$

$$\boldsymbol{L}_{123} p[i_{123}] + \boldsymbol{R}_{123} i_{123} + v_{C_b} \mathbb{I}_3 \bar{u} = Q_{123}, \tag{23}$$

$$L_f \mathbb{I}_3 p[i_f] + r_f \mathbb{I}_3 i_f - (1/2) v_{C_b} \mathbb{I}_3 s = -e_n, \tag{24}$$

where $\boldsymbol{L}_{123} = \mathrm{diag}(L_1, L_2, L_3)$, $\boldsymbol{R}_{123} = \mathrm{diag}(r_{pv}, r_b, r_{sc})$, $Q_{123} = [E_{pv}, E_b, E_{sc}]^\top$, and $p[\cdot]$ is the operator d/dt.

Before continuing, we analyse the EL model in further detail. The first and third term in the left-hand side of (22) represent the current flowing through the bus capacitor and the DC load, respectively. The second term is the current taken by the inverter and the remaining term describes the sum of currents flowing from the boost and both bidirectional converters. Both currents are discontinuous due to the switching actions of s and u, respectively. Equations (23) and (24) are the voltage equations that describe the voltage across each inductor of the system. Similarly, both equations contain discontinuous inputs due to s and u.

Finally, we explicit the passivity properties of the EL system. By arranging the parameters in (22)-(24) into the following matrices

$$\mathcal{M} = \text{block diag}(C_b, \boldsymbol{L}),$$

$$\mathcal{R} = \text{block diag}(R_l^{-1}, \boldsymbol{R}),$$

$$\mathcal{J} = \begin{bmatrix} 0 & -\bar{u}_1 & -\bar{u}_2 & -\bar{u}_3 & \frac{1}{2}s_a & \frac{1}{2}s_b & \frac{1}{2}s_c \\ \bar{u}_1 & 0 & 0 & 0 & 0 & 0 & 0 \\ \bar{u}_2 & 0 & 0 & 0 & 0 & 0 & 0 \\ \bar{u}_3 & 0 & 0 & 0 & 0 & 0 & 0 \\ -\frac{1}{2}s_a & 0 & 0 & 0 & 0 & 0 & 0 \\ -\frac{1}{2}s_b & 0 & 0 & 0 & 0 & 0 & 0 \\ -\frac{1}{2}s_c & 0 & 0 & 0 & 0 & 0 & 0 \end{bmatrix},$$

one deduces the matrix representation

$$\mathcal{M}\dot{w} + \mathcal{J}(s,u)w + \mathcal{R}w = \mathcal{Q}, \tag{25}$$

where $\mathcal{M}$ is a positive-definite diagonal matrix, $\mathcal{R}$ is the dissipation matrix and $\mathcal{J}$ is the interconnection matrix. The total energy function is $\mathcal{H} =$

$\mathcal{T} + \mathcal{V} = (1/2)w^\top \mathcal{M} w$, which satisfies the following energy balance equation

$$\mathcal{H}(T) - \mathcal{H}(0) + \int_0^T w^\top \mathcal{R} w dt = \int_0^T w^\top \mathcal{Q} dt. \tag{26}$$

This equation describes that the sum of the stored energy and dissipated energy equals the supplied energy. Furthermore, if the supplied energy is zero, i.e. $\mathcal{Q} = 0$, the energy is not increasing, hence the equilibrium point of the unforced system is stable.

3.1. Inverter EL model in rotating d-q frame

In this subsection, we derive the EL model of the VSI in the *dq*-coordinates using the Blondel-Park's transform. This transformation produces a change of variables that reduces the complexity of the EL model in its original coordinates. In the new set of coordinates, the definitions of active and reactive power delivered to the AC load by the VSI are more transparent, hence easier to control since the control objective may then be simplified to a set-point regulation problem [18].

A change of variables that formulates a transformation of the 3-phase variables to the dq reference frame may be expressed as $\boldsymbol{f}_{qd0} = K \boldsymbol{f}_{abc}$ [19], where

$$K = \frac{2}{3} \begin{bmatrix} \cos(\phi) & \cos(\phi - 2\pi/3) & \cos(\phi - 4\pi/3) \\ \sin(\phi) & \sin(\phi - 2\pi/3) & \sin(\phi - 4\pi/3) \\ 1/2 & 1/2 & 1/2 \end{bmatrix}, \tag{27}$$

$$\dot{\phi} = \omega = 2\pi 50\text{Hz}. \tag{28}$$

After performing the Blondel-Park's transform on (22) and (24), the EL model of the system with the inverter described in the rotating dq frame is

$$C_b\dot{v}_{C_b} + \frac{1}{2}s^\top J_2 i_f + v_{C_b}R_l^{-1} - \bar{u}^\top i_{123} = 0, \tag{29}$$

$$\boldsymbol{L}_{123}p[i_{123}] + \boldsymbol{R}_{123}i_{123} + v_{C_b}\mathbb{I}_3\bar{u} = Q_{123}, \tag{30}$$

$$\frac{3}{2}\left(L_f\mathbb{I}_3 p[i_f] + J_1 i_f - \frac{1}{2}v_{c_b}\mathbb{I}_3 s + r_f\mathbb{I}_3 i_f\right) = -\frac{3}{2}e_n, \tag{31}$$

where, with some abuse of notation, we define $e_n = [0, E_m, 0]^\top$, $s = [s_q, s_d, s_0]^\top$, $i_f = [i_q, i_d, i_0]^\top$,

$$J_1 = \begin{bmatrix} 0 & \omega L_f & 0 \\ -\omega L_f & 0 & 0 \\ 0 & 0 & 0 \end{bmatrix}, \; J_2 = \begin{bmatrix} 3/2 & 0 & 0 \\ 0 & 3/2 & 0 \\ 0 & 0 & 3 \end{bmatrix}. \tag{32}$$

E_m is the peak voltage of the ideal AC voltage source.

Omitting the homopolar component, in expanded form we have

$$C_b\dot{v}_{C_b} + \frac{3}{4}s^\top i_f + v_{C_b}R_l^{-1} - \bar{u}^\top i_{123} = 0, \tag{33}$$

$$L_1\frac{di_1}{dt} + r_{pv}i_1 + (1-u_1)v_{C_b} = E_{pv}, \tag{34}$$

$$L_2\frac{di_2}{dt} + r_b i_2 + (1-u_2)v_{C_b} = E_b, \tag{35}$$

$$L_3\frac{di_3}{dt} + r_{sc}i_3 + (1-u_3)v_{C_b} = E_{sc}, \tag{36}$$

$$\frac{3}{2}L_f\frac{di_q}{dt} + \frac{3}{2}\omega L_f i_d - \frac{3}{4}s_q v_{C_b} + \frac{3}{2}r_f i_q = 0, \tag{37}$$

$$\frac{3}{2}L_f\frac{di_d}{dt} - \frac{3}{2}\omega L_f i_q - \frac{3}{4}s_d v_{C_b} + \frac{3}{2}r_f i_d = -\frac{3}{2}E_m. \tag{38}$$

We define $i_E = \frac{3}{4}s^\top i_f$ as the current taken from the DC bus by the VSI.

The matrix form of the new system is

$$\overline{\mathcal{M}}\dot{z} + \overline{\mathcal{J}}(s,u)z + \overline{\mathcal{R}}z = \overline{\mathcal{Q}}, \tag{39}$$

where

$$
\begin{aligned}
z &= [v_{C_b}, i_1, i_2, i_3, i_q, i_d]^\top, \\
\overline{\mathcal{M}} &= \text{block diag}(C_b, \boldsymbol{L}_{123}, (3/2)L_f\mathbb{I}_2), \\
\overline{\mathcal{R}} &= \text{block diag}(R_l^{-1}, \boldsymbol{R}_{123}, (3/2)r_f\mathbb{I}_2), \\
\overline{\mathcal{Q}} &= [0, Q_{123}^\top, 0, -(3/2)E_m]^\top, \\
\overline{\mathcal{J}} &= \begin{bmatrix} 0 & -\bar{u}_1 & -\bar{u}_2 & -\bar{u}_3 & \frac{3}{4}s_q & \frac{3}{4}s_d \\ \bar{u}_1 & 0 & 0 & 0 & 0 & 0 \\ \bar{u}_2 & 0 & 0 & 0 & 0 & 0 \\ \bar{u}_3 & 0 & 0 & 0 & 0 & 0 \\ -\frac{3}{4}s_q & 0 & 0 & 0 & 0 & \frac{3}{2}\omega L_f \\ -\frac{3}{4}s_q & 0 & 0 & 0 & -\frac{3}{2}\omega L_f & 0 \end{bmatrix}.
\end{aligned}
$$

Analogously, the total energy function is $\overline{\mathcal{H}} = (1/2)z^\top\overline{\mathcal{M}}z$ and one can easily arrive at a similar energy balance equation as (26) with the same passivity properties.

The EL model (39) and its equivalent in the original reference frame (25) contain discontinuous input terms due to the switching actions of the bipolar switching functions s and u. Thus, the analysis of their solutions and also the controller design are difficult tasks. A suitable way of addressing this problem is deriving an average model of the system. The average model behaves exactly as the switched model under extreme duty ratios saturation conditions and under intermediary duty ratio conditions it is consistent with the physically plausible interpretation of the averaged values of its currents and voltages. The average model of the system does not alter the structure of the nonlinear EL model but now the state vector z represents the averaged state vector and the switching functions s and u are regarded as duty ratio functions with values in their appropriate interval. From this point forward, we will define the average model of the HGS by equations (33)-(38) or by its matrix form (39).

We conclude this section describing mathematically the interaction of the system with the AC voltage source and the AC load. Observing the HGS structure (Figure 1), the network equations are given by Kirchhoff's laws

$$i_n + i_f - i_z = 0, \quad e_n = e_z, \tag{40}$$

where e_z is the voltage across the generic impedance Z.

4. Passivity-based controller design

PBC is a methodology to design controllers for physical systems modifying its total energy function and damping characteristics [20]. The central idea of the PBC methodology is to achieve a closed-loop system dynamics associated to a closed-loop desired energy function of the form

$$\mathcal{H}_d = (1/2)\tilde{z}^\top \overline{\mathcal{M}} \tilde{z}, \tag{41}$$

where its election is motivated by the form of the total energy function $\overline{\mathcal{H}}$ of the average model. Let $z_d = [v_{C_b d}, i_{1d}, i_{2d}, i_{3d}, i_{qd}, i_{dd}]^\top$ denote the desired state vector of the closed-loop system, thus we define the error state vector $\tilde{z}$, which we want to drive to zero, as $\tilde{z} = z - z_d = [\tilde{z}_{C_b}, \tilde{z}_1, \tilde{z}_2, \tilde{z}_3, \tilde{z}_q, \tilde{z}_d]^\top$. Since the system is underactuated we cannot select arbitrary functions for the desired state signals, they will thus result from the definition of the error dynamics.

The election of $\mathcal{H}_d$ gives the following error dynamics equation

$$\overline{\mathcal{M}}\dot{\tilde{z}} + \overline{\mathcal{J}}(s,u)\tilde{z} + \mathcal{R}_d\tilde{z} = 0, \tag{42}$$

where we have added a desired damping by choosing

$$\mathcal{R}_d = \overline{\mathcal{R}} + \mathcal{R}_1, \tag{43}$$

where $\mathcal{R}_1 = \mathrm{diag}(r_{C_b}, r_1, r_2, r_3, r_q, r_d)$ with each diagonal element positive. Taking the derivative of $\mathcal{H}_d$ along the solutions of (42) we get

$$\dot{\mathcal{H}}_d = -\tilde{z}^\top \mathcal{R}_d \tilde{z} \leq -\frac{\alpha}{\beta}\mathcal{H}_d < 0, \quad \forall \tilde{z} \neq 0, \tag{44}$$

where α may be chosen to be $\alpha = \min(\mathcal{R}_d)$ and $\beta = \max(\frac{1}{2}\overline{\mathcal{M}})$. Therefore, the error dynamics is exponentially stable.

From (42) and using (39) we obtain

$$\overline{\mathcal{M}}\dot{z}_d + \overline{\mathcal{J}}(s,u)z_d + \mathcal{R}_d z_d - \mathcal{R}_1 z = \overline{\mathcal{Q}}, \tag{45}$$

where this equation is explicitly written as

$$C_b\dot{v}_{C_bd} + \frac{3}{4}s^\top i_{fd} + \frac{v_{C_bd}}{R_l} - \bar{u}^\top i_{123d} - r_{C_b}\tilde{z}_{C_b} = 0, \tag{46}$$

$$L_1\frac{di_{1d}}{dt} + r_{pv}i_{1d} + (1-u_1)v_{C_bd} - r_1\tilde{z}_1 = E_{pv}, \tag{47}$$

$$L_2\frac{di_{2d}}{dt} + r_b i_{2d} + (1-u_2)v_{C_bd} - r_2\tilde{z}_2 = E_b, \tag{48}$$

$$L_3\frac{di_{3d}}{dt} + r_{sc}i_{3d} + (1-u_3)v_{C_bd} - r_3\tilde{z}_3 = E_{sc}, \tag{49}$$

$$\frac{3}{2}L_f\frac{di_{qd}}{dt} + \frac{3}{2}\omega L_f i_{dd} - \frac{3}{4}s_q v_{C_bd} + \frac{3}{2}r_f i_{qd} - r_q\tilde{z}_q = 0, \tag{50}$$

$$\frac{3}{2}L_f\frac{di_{dd}}{dt} - \frac{3}{2}\omega L_f i_{qd} - \frac{3}{4}s_d v_{C_bd} + \frac{3}{2}r_f i_{dd} - r_d\tilde{z}_d = -\frac{3}{2}E_m. \tag{51}$$

The equations (46)-(51) implicitly define the controller of the system. To obtain an explicit expression we must use the degrees of freedom to match the number of equation and variables. Since direct voltage control is infeasible due to lack of stability [21], this goal is achievable through the regulation of the inductor currents. Therefore, we establish reference values for the desired current of each inductor adding five new equations. These are $i_{1d} = i_{1*}$, $i_{2d} = i_{2*}$, $i_{3d} = i_{3*}$, $i_{qd} = i_{q*}$ and $i_{dd} = i_{d*}$, where the reference values are yet to be defined. We establish that the notation $(\cdot)_*$ is used exclusively for external reference signals, while $(\cdot)_d$ denotes signals generated by the controller. Hence, the reference signal for the desired current of each inductor is given externally and the signal reference for the desired dc voltage is defined by the PBC.

From (47)-(51) the control variables u and s can be solved as follows:

$$u_1 = 1 - \frac{1}{v_{C_bd}} \left(E_{pv} - r_{pv} i_{1d} + r_1 \tilde{z}_1 \right), \tag{52}$$

$$u_2 = 1 - \frac{1}{v_{C_bd}} \left(E_b - r_b i_{2d} + r_2 \tilde{z}_2 \right), \tag{53}$$

$$u_3 = 1 - \frac{1}{v_{C_bd}} \left(E_{sc} - r_{sc} i_{3d} + r_3 \tilde{z}_3 \right), \tag{54}$$

$$s_q = \frac{1}{v_{C_bd}} \left(2\omega L_f i_{dd} + 2 r_f i_{qd} - \frac{4}{3} r_q \tilde{z}_q \right), \tag{55}$$

$$s_d = \frac{1}{v_{C_bd}} \left(2E_m - 2\omega L_f i_{qd} + 2 r_f i_{dd} - \frac{4}{3} r_d \tilde{z}_d \right). \tag{56}$$

Then, substituting u and s into (46) and after a straightforward calculation, the controller state v_{C_bd} is:

$$\dot{v}_{C_bd} = \frac{1}{C_b} \left(-\frac{3}{4} s^\top i_{fd} - \frac{v_{C_bd}}{R_l} + \bar{u}^\top i_{123d} + r_{C_b} \tilde{z}_{C_b} \right). \tag{57}$$

5. Energy management strategy

In this section, we define an adequate energy management strategy (EMS) to efficiently command each component of the HGS. The EMS should ensure that the HGS supplies the required load power demand, subjected to the constraints imposed by the different components under varying atmospheric conditions. Also, the EMS is intended to exploit the renewable resources avoiding the use of the grid as energy source.

There are several approaches in the literature to address the energy management in hybrid power systems. In this sense, a comprehensive review is done in [22]. EMS can be classified into two main categories: i) classical strategies and ii) intelligent strategies. In the first category we can find strategies based on heuristic rules [23, 24, 25] or filtration [26, 27], while in the second category strategies based on fuzzy logic [28], model predictive control [29, 30], receding horizon approach [31, 32], multi-agent based power [33], Pontryagin's minimum principle [34], dynamic programming [35] or nonlinear programming [36] are reported. Heuristic based strategies are more appropriate to work in real time and for this reason we prefer to use this kind of strategy in this work.

In this work, the EMS is formalized using a finite-state machine approach [25]. The state machine is composed of states in which a specific mode of operation of the system is defined. The change from one state to another is called a transition and this occurs when a condition defining the transition is true. A finite-state machine can be graphically depicted by a statechart, which is a schematic diagram where the states are typically represented as circles connected between each others through transitions represented by arrows. Each arrow has attached an event that produces the transition [37].

In this section, we design an EMS using a state machine in which each state defines the reference currents needed by the passivity-based controller and the transition conditions or events are defined from comparison rules using process variables such as state of charge, current, power, etc. This state machine is presented by the statechart depicted in Figure 2, which can be defined by a tuple EMS $= \langle S, \Sigma, \epsilon, s_0 \rangle$, where

- $S = \{s_1, s_2, s_3, s_4, s_5\}$ is the set of all states in the statechart.
- $\Sigma = \{1, \cdots, 9\}$ is the set of possible input events (defined in Table 2).
- ϵ is a function that maps states and input events to states ($\epsilon : S \times \Sigma \to S$).
- $s_0 \in S$ is the initial state. In this case, $s_0 = s_1$.

The proposed EMS maximizes the power generation from the solar energy system, thus the reference current i_{1*} is defined by a maximum power point tracking (MPPT) algorithm. That is, $i_{1*} = f_{MPPT}(T, \lambda)$. Also, this EMS only provides the active power of the AC load, therefore, we set $i_{q*} = 0$. Since both definitions are common to all states in the EMS statechart they are not stated in the following description of each state in the set S. A detailed description of each current reference definition could be found in Appendix A.

State 1 (Energy sale mode): The solar energy system is capable of satisfying the demand, recharging the battery and supercapacitor banks, if it is necessary, and selling the remaining energy to the grid:

$$i_{2*} = i_b^c, \tag{58}$$

$$i_{3*} = i_{sc}^c, \tag{59}$$

$$i_{d*} = (1/s_d)\left((4/3)i_{Ed} - s_q i_{qd}\right), \tag{60}$$

where $i_{Ed} = \bar{u}^\top i_{123} - v_{C_b}^* R_l^{-1}$ is the necessary current taken by the inverter in order to satisfy the AC load power demand and sell the surplus to the grid. i_b^c and i_{sc}^c are the reference charging currents for the battery and supercapacitor banks, respectively. In this work, we define them considering the SOC. If the SOC is sufficiently high, the reference charging current is set to zero, else the storage elements are charged at their nominal values $i_x^{c,n}$ (Figure 3).

State 2 (Self-sufficient mode): The solar energy system and the storage system are capable of satisfying the demand without energy transaction with the grid. This mode covers several situations from satisfying the load power demand with the solar energy system and storing the surplus, to non-existent solar energy generation with the storage system supplying the totally of the load power demand:

$$i_{2*} = \left(-\bar{u}_1 i_1 + i_E + v_{C_b}^* R_l^{-1}\right) / \bar{u}_2, \tag{61}$$

$$i_{3*} = \left(-\bar{u}_1 i_1 - \bar{u}_2 i_2 + i_E + v_{C_b}^* R_l^{-1}\right) / \bar{u}_3, \tag{62}$$

$$i_{d*} = i_{zd}. \tag{63}$$

It is important to note that the storage reference currents are limited by the constraints imposed by (10).

State 3 (Critical mode): When one of the storage elements reaches a minimum SOC the system replaces the storage system power supply with the grid power supply to meet the load requirements:

$$i_{2*} = 0, \tag{64}$$

$$i_{3*} = 0, \tag{65}$$

$$i_{d*} = (1/s_d)\left((4/3) i_{Ed} - s_q i_{qd}\right). \tag{66}$$

State 4 (Maximum capacity mode): When the load power demand exceeds the power capacity of the system, the grid provides the rest:

$$i_{2*} = i_b^d, \tag{67}$$

$$i_{3*} = i_{sc}^d, \tag{68}$$

$$i_{d*} = (1/s_d)\left((4/3)i_{Ed} - s_q i_{qd}\right). \tag{69}$$

Similarly, i_b^d and i_{sc}^d are the reference discharging currents for the battery and supercapacitor banks, respectively. In this case, there is a hysteresis to recover the SOC until certain point without discharging the storage elements during the recovery process (Figure 3).

State 5 (Recovery mode): When the energy generated from the solar energy system exceeds the load requirements, this surplus is used to charge those storage elements in critical conditions to restore their SOC until certain level:

$$i_{2*} = \left(-\bar{u}_1 i_1 - c\bar{u}_3 i_3 + i_E + v_{C_b}^* R_l^{-1}\right)/\bar{u}_2, \tag{70}$$

$$i_{3*} = \left(-\bar{u}_1 i_1 - \bar{c}\bar{u}_2 i_2 + i_E + v_{C_b}^* R_l^{-1}\right)/\bar{u}_3, \tag{71}$$

$$i_{d*} = i_{zd}, \tag{72}$$

where if $SOC_b > SOC_b^{OK}$, then $c = 1$, else $c = 0$. The purpose of the binary variable c is to establish a preference between both storage elements to charge the one in most critical condition. If both elements have their SOC under critical conditions, the battery bank has main priority; hence we define c as a function of SOC_b.

The events are defined in Table 2. Event 1 produces the transition from s_1 to s_2 when the energy generated is not sufficient enough to satisfy the

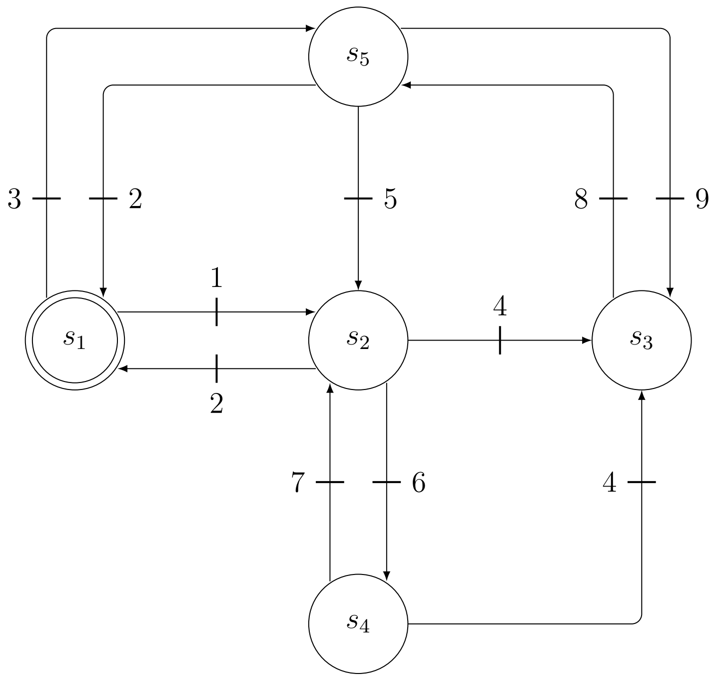

Figure 2: Schematic diagram of the energy management strategy.

load and storage requirements. This situation is detected by a positive value in the grid power P_n. δ is a sufficiently small value of power to avoid the zero crossing. Event 3 is very similar to Event 1, but for the critical state of the storage elements. Events 2 and 6 are identical but the former becomes active when the storage system reaches its maximum charging capacity and the latter when it reaches its maximum discharging capacity, considering a small tolerance in both cases. Event 7 is analogous to events 1 or 3 but now the event becomes active when a negative value in the grid power is detected, indicating that the assistance from the grid is not longer necessary. Event 4 indicates that either the battery bank or the supercapacitor bank have their SOC under a critical level. Event 5 becomes active after the SOC of the storage system in critical condition has been restored. Finally, events 8 and 9 compare the power generated by the PV system with the load power demand to charge the storage elements when there is energy available.

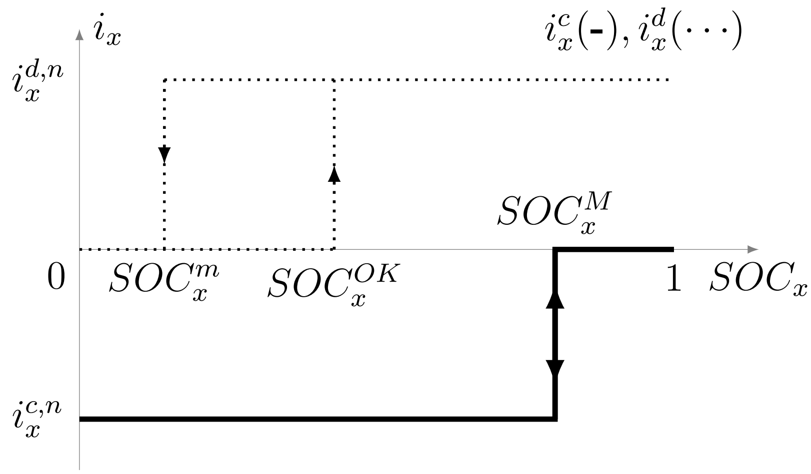

Figure 3: Charge and discharge reference current. $x = b, sc$.

6. Simulations and results

In this section, we test the designed passivity-based controller with the proposed EMS. We use ambient temperature and insolation data for a typical winter day (July 17, 2009) and a typical summer day (January 23, 2009) in Rosario, Argentina to simulate under realistic conditions. Both profiles are shown in Figure 4a and 4b. Also, the load power demand profile (P_l) depicted in Figure 4c corresponds to a residential hourly average power consumption.

6.1. System sizing

Before testing the behaviour of the system we size and parametrize each system component. The sizing of renewable hybrid systems is a complex issue because there is a compromise between cost and reliability, coupled with the uncertainty in demand and energy production. The bibliography in this matter is extensive [38]-[46]. In this section, we proposed a reasonable sizing in order to test the controller design and the energy management strategy.

The nominal voltage value for the DC bus is $v_{C_b}^{*} = 100V$. We set the number of PV cells in series and in parallel as $n_s^{pv} = 50$ and $n_p^{pv} = 38$, respectively. The parameters used for the lead-acid battery bank are given in Table 3 and the battery bank is formed of $n_s^b = 4$ and $n_p^b = 10$. In the case of the SC bank, we used one unit with the features given in Table 4.

Finally, the specifications of the power converters are given in Table 5.

6.2. Simulation tests

The mathematical model of the HGS defined in (39) as well as the control laws (52)-(57) and the EMS are implemented in language Modelica using OpenModelica [47]. We simulate the proposed HGS using the winter and summer weather profiles with their respective winter and summer load power demand and under same initial conditions.

First, the system is evaluated with the winter weather profile and with the following initial state of charge: $SOC_b^{init} = 0.75$ and $SOC_{sc}^{init} = 0.8$. The voltage of the DC bus is shown in Figure 5 where it can be seen that the system achieves a very good regulation throughout the simulation. Figure 9 shows the power exchanged by each component of the system. During the first 5.5 hours the storage elements are capable of supplying the power demanded by the loads (P_l) establishing the operation mode of the EMS in the state s_2 as it is shown in Figure 6. The currents of the storage elements are depicted in Figure 8. The battery bank supplies the totally of the load power demand and the supercapacitor bank only delivers power due to tracking mismatches. The current of the supercapacitor bank could be observed by the zoom in Figure 8. Continuing with the description of the simulation, in Figure 7 the SOC_b reaches a critical point ($SOC_b^m = 0.4$) due to the lack of energy available from the PV arrays, and the EMS makes a transition to state s_3. The grid replaces the role of the storage elements avoiding its depletion. Thus, the grid power P_n matches the load power P_l until the PV arrays start transforming solar energy into electric energy. This increment in the power generation from the PV arrays reduces the grid energy consumption to zero. Having reached this point, the EMS transitions to state s_5 recovering the battery. When the SOC_b is higher than a reasonable level ($SOC_b^{OK} = 0.5$), the EMS leaves the recovery mode transitioning again to state s_2. Since the generated power P_{pv} is still increasing, the system reaches its maximum storage capacity sending the surplus to the grid, that is, selling energy (State 1). Then, with the storage elements fully charged ($SOC_{b,sc} = 0.8$) and the decreasing insolation, the systems transitions to the self-sufficient mode (s_2) meeting the power requirements without assistance from the grid. This mode of operation persists until the load power demand exceeds the power capacity of the HGS, transitioning to s_4 where the grid supports the HGS to meet the load power demand. A transition period between states s_3 and s_4 occurs until finally the load power demand is high enough to establish the EMS in state s_4. The simulation ends with both storage elements with low SOC, transitioning the EMS to state s_3.

Finally, we simulate the system with the summer weather data and summer load power demand with identical initial conditions than before. Figures 10-14 includes the simulation responses of many variables of interest. Although more energy is available from the renewable source, the summer load power profile is also more demanding. Therefore, the HGS is slightly more self-sufficient than in the previous simulation. For instance, the state s_1 is active a longer period of time during daylight, but at the beginning of the simulation the SOC of the battery bank reaches the minimum value sooner than before. The time in recovery mode (s_5) is also shorter in this new simulation. A quantitative comparison could be made between both simulations after introducing the following concept.

A reliable electrical power system can be defined as a system capable to feed the load demand with a small loss of power supply probability (LPSP) [48]. LPSP is defined as the probability that the hybrid system is unable to satisfy the load demand. A LPSP of 0 means the load is always satisfied whereas a LPSP of 1 means the contrary. The objective function LPSP can be expressed as follows:

$$\mathrm{LPSP} = \frac{T_{ft}}{T_t}, \tag{73}$$

where T_t is the total time of weather data used in the analysis and T_{ft} is the power failure time, which is defined as the time that the load is not satisfied. Since the HGS is coupled with the grid, the load power demand is ensured all the time; hence the traditional definition of the LPSP renders useless. Instead, we proposed to evaluate the LPSP by means of the reliability of the system working without the support of the grid. Thus, we define T_{ft} as the period of time in which the active power from the grid is positive, that is, when the HGS needs energy from the grid. Therefore, the definition of T_{ft} is the following:

$$T_{ft} = \int_0^{T_t} \gamma(t)dt, \tag{74}$$

where

$$\gamma(t) = \begin{cases} 1 & \text{if } P_n > 0, \\ 0 & \text{otherwise.} \end{cases} \tag{75}$$

Evaluating the LPSP in both scenarios gives 0.375 and 0.369 using the winter and summer weather profile, respectively. The results show that both LPSPs are high, concluding that the sizing prioritizes the overall cost rather than the system reliability. In a grid-connected power system, the grid acts like a battery with an unlimited storage capacity. So it could handle seasonal load variations. Thus, the sizing of the storage elements could be reduced, which explains the high LPSP values obtained in both simulations.

7. Conclusions

We have presented an energy management strategy integrated with a passivity-based controller for a hybrid generation system. The hybrid system consists of two types of storage elements (one with high specific energy and the other with high specific power), one source of renewable energy (solar) and DC and AC loads. Also, the system is coupled with an electrical network which allows an exchange of energy between them. These power elements are connected to a DC bus through power converters. We obtained an Euler-Lagrange model based on the kinetic co-energy and the potential energy of the power system. Subsequently, we designed the passivity-based controllers to command the power converters. Finally, a energy management strategy establishes the reference signals of the controller.

We validate the performance of the strategy by means of computer simulations using different weather and load data profiles. We compare both simulations in terms of loss of power supply probability (LPSP), resulting in that both scenarios present similar LPSP values. The results obtained indicate feasibility of the proposed control technique and energy management strategy. Finally, although the study is intended for one particular system, the proposed controller design methodology is applicable for other hybrid systems with multiple renewable sources. It is within our interests to extend this work to include a wind energy system. Also, an optimal sizing methodology for designing the overall hybrid system is the subject of on-going research.

Acknowledgement

The authors thank the financial support of CONICET (National Scientific and Technical Research Council), UNR-FCEIA (Rosario National University), ANPCyT PICT 2014-1607 (Agencia Nacional de Promoción Científica y Técnica) from Argentina and PIP 0211, CONICET, Argentina.

Appendix A.

Here, we briefly describe the procedure to obtain the definition of each reference current presented in the description of the EMS states in Section 5.

The main purpose of the Passivity-Based controller is to regulate the voltage of the DC bus. As we have mentioned before, this objective is only feasible through indirect voltage regulation. This means that the DC voltage regulation can be indirectly accomplished by a suitable definition of each reference current i_{2*}, i_{3*} and i_{d*}. The regulation of the DC voltage implies that equation (33) holds with $v_{C_b} = v_{C_b}^*$ and $\dot{v}_{C_b} = 0$. That is,

$$\frac{3}{4} s^\top i_f + v_{C_b}^* R_l^{-1} - \bar{u}^\top i_{123} = 0. \tag{A.1}$$

Therefore, the definition of the reference currents will be obtained from (A.1).

In each EMS state the system defines the reference current of only one element to regulate the DC voltage. For instance, in state s_1, s_3 and s_4 the PBC regulates the DC voltage by means of the inverter. For ease of reference, we write again the equation (60):

$$i_{d*} = (1/s_d)\left((4/3) i_{Ed} - s_q i_{qd}\right), \tag{A.2}$$

$$i_{Ed} = \bar{u}^\top i_{123} - v_{C_b}^* R_l^{-1}. \tag{A.3}$$

i_{Ed} is the desired inverter current that regulates the DC bus, then (A.3) is obtained from (A.1). Finally, i_{d*} is derived from the expression of the inverter current

$$\frac{3}{4} s^\top i_f = i_E. \tag{A.4}$$

When the state is s_2 or s_5, the regulation task is accomplished by the definition of the reference current of the storage elements. For example, in state s_2 these definitions are:

$$i_{2*} = \left(-\bar{u}_1 i_1 + i_E + v_{C_b}^* R_l^{-1}\right) / \bar{u}_2, \tag{A.5}$$

$$i_{3*} = \left(-\bar{u}_1 i_1 - \bar{u}_2 i_2 + i_E + v_{C_b}^* R_l^{-1}\right) / \bar{u}_3. \tag{A.6}$$

Both (A.5) and (A.6) are derived from (A.1) but the former neglects the effect of the other storage element over the DC bus ($-\bar{u}_3 i_3$). The consequence of this is that once the controller has reached the equilibrium point, the regulation task will be accomplished by the definition of i_{2*} with $i_{3*} = 0$, that is, only the battery bank will play an active role in the regulation of the DC bus leaving the supercapacitor bank in stand by. But if i_{2*} reaches its extreme value imposed by the constraint in (10), then i_{3*} will assumed the required value to regulate the DC voltage. This situation is similar to state s_5 but in (70) and (71) we introduce the binary variable c to invert the behaviour when it is necessary.

References

[1] Y. Mohammed, M. Mustafa, N. Bashir, Hybrid renewable energy systems for off-grid electric power: Review of substantial issues, Renewable and Sustainable Energy Reviews 35 (2014) 527–539.

[2] D. Kaundinya, P. Balachandra, N. Ravindranath, Grid-connected versus stand-alone energy systems for decentralized power–A review of literature, Renewable and Sustainable Energy Reviews 13 (2009) 2041–2050.

[3] F. Valenciaga, P. Puleston, P. Battaiotto, R. Mantz, Passivity/sliding mode control of a stand-alone hybrid generation system, IEE Proc. Control Theory Appl. 147(6) (2000) 680–686.

[4] D. Pavković, M. Lobrović, M. Hrgetić, A. Komljenović, A design of cascade control system and adaptive load compensator for bat-

tery/ultracapacitor hybrid energy storage-based direct current microgrid, Energy Conversion and Management 114 (2016) 154–167.

[5] H. Fakham, D. Lu, B. Francois, Power control design of a battery charger in a hybrid active PV generator for load-following applications, IEEE Trans. Industrial Electronics 58(1) (2011) 892–902.

[6] R. Ortega, A. van der Schaft, I. Mareels, B. Maschke, Putting energy back in control, IEEE Control Syst. Mag. 21(2) (2001) 18–33.

[7] R. Ortega, A. Van Der Schaft, B. Maschke, G. Escobar, Interconnection and damping assignment passivity-based control of port-controlled hamiltonian systems, Automatica 38(4) (2002) 585–596.

[8] R. Ortega, P. Nicklasson, G. Espinosa-Pérez, On speed control of induction motors, Automatica 32(3) (1996) 455–460.

[9] C. Batlle, A. Dòria-Cerezo, R. Ortega, Power flow control of a doubly-fed induction machine coupled to a flywheel, European Journal of Control 11 (2005) 209–221.

[10] K. Yokoyama, M. Takahashi, Passivity-based nonlinear stabilizing control for a mobile inverted pendulum, in: ICINCO 2011 - Proceedings of the 8th International Conference on Informatics in Control, pp. 128–134.

[11] M. Ayad, M. Becherif, A. Hennin, A. Aboubou, M. Wack, S. Laghrouche, Passivity-based control applied to DC hybrid power source using fuel cell and supercapacitors, Energy Conversion and Management 51 (2010) 1468–1475.

[12] C. Lungoci, M. Becherif, A. Miraoui, E. Helerea, On board energy system based on batteries and supercapacitors, in: IFAC Workshop ICPS'07, Cluj-Napoca, Rumania.

[13] A. Tofighi, M. Kalantar, Power management of PV/battery hybrid power source via passivity-based control, Renewable Energy 36 (2011) 2440–2450.

[14] C. Batlle, A. Dòria-Cerezo, E. Fossas, Bidirectional power flow control of a power converter using passive hamiltonian techniques, Circuit Theory and Applications 36(7) (2008) 769–788.

[15] F. Valenciaga, P. Puleston, Power control of a photovoltaic array in a hybrid electric generation system using sliding mode techniques, IEE Proc. Control Theory Appl. 148(6) (2001) 448–455.

[16] V. Salas, E. Olías, A. Barardo, A. Lázaro, Review of maximum power point tracking algorithms for stand-alone photovoltaic systems, Solar Energy Materials and Solar Cells 90 (2006) 1555–1578.

[17] O. Tremblay, L. Dessaint, Experimental validation of a battery dynamic model for EV applications, World Electric Vehicle Journal 3 (2009) 284–289.

[18] L. Tzann-Shin, Lagrangian modeling and passivity-based control of three-phase AC/DC voltage-source converters, IEEE Trans. Industrial Electronics 51(4) (2004) 892–902.

[19] P. Krause, O. Wasynczuk, S. Sudhoff, Analysis of Electric Machinery and Drive Systems, IEEE Press, Wiley, New York, 2nd edition, 2002.

[20] R. Ortega, G. Espinosa-Pérez, A. Astolfi, Passivity-based control of AC drives: theory for the user and application examples, International Journal of Control 86 (2013) 625–635.

[21] R. Ortega, A. Loría, P. Nicklasson, H. Sira-Ramírez, Passivity-based Control of Euler-Lagrange Systems. Mechanical, Electrical and Electromechanical Applications, Springer-Verlag, London, 1998.

[22] L. Olatomiwa, S. Mekhilef, M. Ismail, M. Moghavvemi, Energy management strategies in hybrid renewable energy systems: A review, Renewable and Sustainable Energy Reviews 62 (2016) 821–835.

[23] J. Morales-Morales, I. Cervantes, U. Cano-Castillo, On the design of robust energy management strategies for fchev, IEEE Transactions on Vehicular Technology (2013).

[24] M. Sorrentino, C. Pianese, M. Maiorino, An integrated mathematical tool aimed at developing highly performing and cost-effective fuel cell hybrid vehicles, Journal of Power Sources 221 (2013) 308–317.

[25] D. Feroldi, L. Nieto Degliuomini, M. Basualdo, Energy management of a hybrid system based on windsolar power sources and bioethanol, Chemical Engineering Research and Design 91 (2013) 1440–1455.

[26] A. M. Gee, F. V. Robinson, R. W. Dunn, Analysis of battery lifetime extension in a small-scale wind-energy system using supercapacitors, IEEE Transactions on Energy Conversion 28 (2013) 24–33.

[27] Y. Song, Q. Cao, X. Du, H. R. Karimi, Control strategy based on

wavelet transform and neural network for hybrid power system, Journal of Applied Mathematics 2013 (2013).

[28] M. Kisacikoglu, M. Uzunoglu, M. Alam, Load sharing using fuzzy logic control in a fuel cell/ultracapacitor hybrid vehicle, International Journal of Hydrogen Energy 34 (2009) 1497–1507.

[29] L. Valverde, C. Bordons, F. Rosa, Integration of fuel cell technologies in renewable-energy-based microgrids optimizing operational costs and durability, IEEE Transactions on Industrial Electronics 63 (2016) 167–177.

[30] A. Arce, A. del Real, C. Bordons, MPC for battery/fuel cell hybrid vehicles including fuel cell dynamics and battery performance improvement, Journal of Process Control 19 (2009) 1289–1304.

[31] X. Wang, H. Teichgraeber, A. Palazoglu, N. El-Farra, An economic receding horizon optimization approach for energy management in the chlor-alkali process with hybrid renewable energy generation, Journal of Process Control 24 (2014) 1318–1327.

[32] D. Feroldi, P. Rullo, D. Zumoffen, Energy management strategy based on receding horizon for a power hybrid system, Renewable Energy 75 (2015) 550–559.

[33] D. Tang, X. Yan, Y. Yuan, K. Wang, L. Qiu, Multi-agent based power and energy management system for hybrid ships, in: 2015 International Conference on Renewable Energy Research and Applications (ICRERA), IEEE, pp. 383–387.

[34] J. Zhao, A. Sciarretta, Design and control co-optimization for hybrid powertrains: Development of dedicated optimal energy management strategy, IFAC-PapersOnLine 49 (2016) 277–284.

[35] D. Fares, R. Chedid, F. Panik, S. Karaki, R. Jabr, Dynamic programming technique for optimizing fuel cell hybrid vehicles, International Journal of Hydrogen Energy 40 (2015) 7777–7790.

[36] L. V. Pérez, E. A. Pilotta, Optimal power split in a hybrid electric vehicle using direct transcription of an optimal control problem, Mathematics and Computers in Simulation 79 (2009) 1959–1970.

[37] F. Schneider, Implementing fault-tolerant services using the state machine approach: A tutorial, ACM Computing Surveys (CSUR) 22 (1990) 299–319.

[38] D. Feroldi, D. Zumoffen, Sizing methodology for hybrid systems based on multiple renewable power sources integrated to the energy management strategy, International Journal of Hydrogen Energy 39 (2014) 8609–8620.

[39] J. P. Fossati, A. Galarza, A. Martín-Villate, L. Fontán, A method for optimal sizing energy storage systems for microgrids, Renewable Energy 77 (2015) 539–549.

[40] C. Liu, L. Liu, Optimal power source sizing of fuel cell hybrid vehicles based on pontryagin's minimum principle, International Journal of Hydrogen Energy (2015).

[41] M. Masih-Tehrani, M.-R. Ha'iri-Yazdi, V. Esfahanian, A. Safaei, Optimum sizing and optimum energy management of a hybrid energy storage system for lithium battery life improvement, Journal of Power Sources 244 (2013) 2–10.

[42] X. Hu, L. Johannesson, N. Murgovski, B. Egardt, Longevity-conscious dimensioning and power management of the hybrid energy storage system in a fuel cell hybrid electric bus, Applied Energy 137 (2015) 913–924.

[43] Y. Eren, H. Gorgun, An applied methodology for multi-objective optimum sizing of hybrid electric vehicle components, International Journal of Hydrogen Energy 40 (2015) 2312–2319.

[44] R. Hosseinalizadeh, H. Shakouri, M. S. Amalnick, P. Taghipour, Economic sizing of a hybrid (PV-WT-FC) renewable energy system (HRES) for stand-alone usages by an optimization-simulation model: Case study of iran, Renewable and Sustainable Energy Reviews 54 (2016) 139–150.

[45] A. Abbassi, M. A. Dami, M. Jemli, A statistical approach for hybrid energy storage system sizing based on capacity distributions in an autonomous PV/wind power generation system, Renewable Energy 103 (2017) 81–93.

[46] S. Mandelli, C. Brivio, E. Colombo, M. Merlo, A sizing methodology based on levelized cost of supplied and lost energy for off-grid rural electrification systems, Renewable Energy 89 (2016) 475–488.

[47] OpenModelica, https://www.openmodelica.org/, 2017.

[48] D. Nelson, M. Nehrir, C. Wang, Unit sizing and cost analysis of stand-alone hybrid wind/PV/fuel cell power generation systems, Renewable Energy 31 (2006) 1641–1656.

Table 1: Parameters used in the solar system.

Parameter	Value
q	$1.6 \times 10^{-19}(C)$
A_c	1.6
K	$1.3805 \times 10^{-23}(NmK^{-1})$
K_l	$0.0017(A\underline{o}C^{-1})$
I_{or}	$2.0793 \times 10^{-6}(A)$
T_{ref}	$301.18(K)$
E_{go}	$1.10(V)$
r_{pv}	$0.5(\Omega)$

Table 2: Events in the set Σ.

Event	Description
1	$P_n > \delta \wedge SOC_b \geq SOC_b^{OK} \wedge SOC_{sc} \geq SOC_{sc}^{OK}$
2	$P_n == 0 \wedge \lvert i_b - i_b^c \rvert \leq 1\% \wedge \lvert i_{sc} - i_{sc}^c \rvert \leq 1\%$
3	$P_n > \delta \wedge \left(SOC_b < SOC_b^{OK} \vee SOC_{sc} < SOC_{sc}^{OK}\right)$
4	$SOC_b \leq SOC_b^m \vee SOC_{sc} \leq SOC_{sc}^m$
5	$SOC_b \geq SOC_b^{OK} \wedge SOC_{sc} \geq SOC_{sc}^{OK}$
6	$P_n == 0 \wedge \lvert i_b - i_b^d \rvert \leq 1\% \wedge \lvert i_{sc} - i_{sc}^d \rvert \leq 1\%$
7	$P_n < -\delta$
8	$P_{pv} - P_{Rl} - P_z > 0$
9	$P_{pv} - P_{Rl} - P_z < 0$

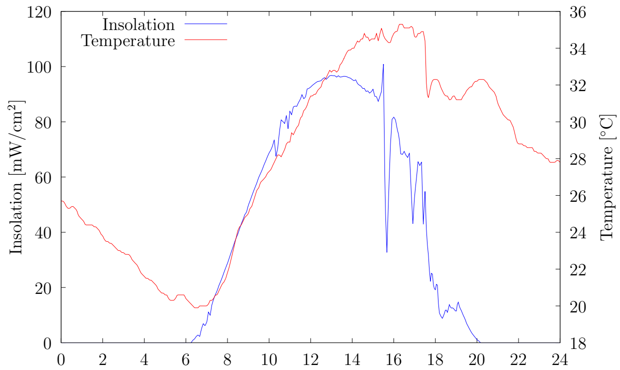

(a) Insolation and temperature profile of a summer day.

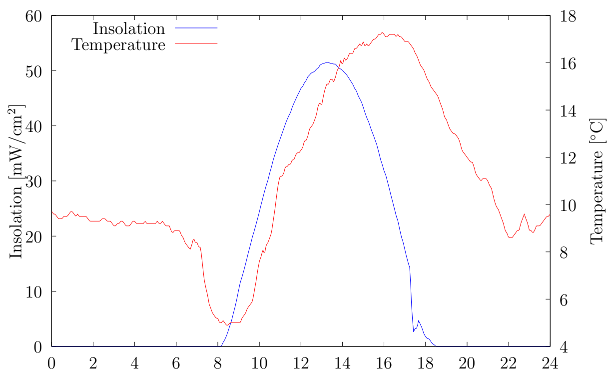

(b) Insolation and temperature profile of a winter day.

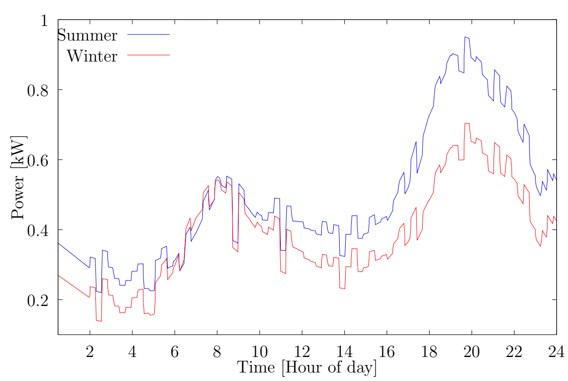

(c) Load power demand profiles.

Figure 4: Simulation results using winter weather profile.

Table 3: Lead-acid battery parameters.

Parameter	Value	Parameter	Value
$E_0(V)$	12.47	$I_b^m(A)$	-1
$K_b(\Omega)$	0.047	$I_b^M(A)$	1
$Q(Ah)$	7.2	$r_b(\Omega)$	0.04
$A(V)$	0.83	$B(Ah^{-1})$	125

Table 4: Supercapacitor parameters.

Parameter	Value
Rated voltage(V)	48
$C_{sc}(F)$	83
$r_{sc}(\Omega)$	0.01
$I_{sc}^m(A)$	-10
$I_{sc}^M(A)$	10

Table 5: Specifications of power converters.

Parameter	Value	Parameter	Value
L_1	$1(mH)$	r_f	$0.5(\Omega)$
L_2	$1(mH)$	C_b	$10000(\mu F)$
L_3	$1(mH)$	R_l	$250(\Omega)$
L_f	$1(mH)$	E_m	220(V)

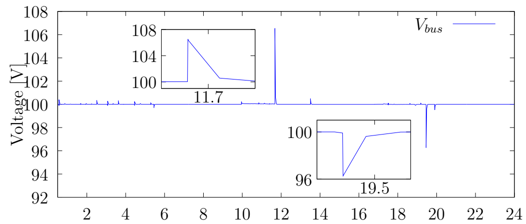

Figure 5: DC bus voltage with winter profile.

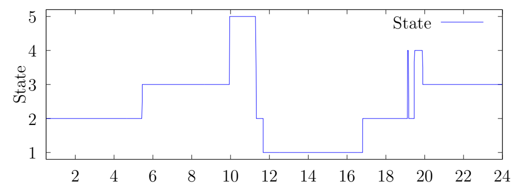

Figure 6: EMS state with winter profile.

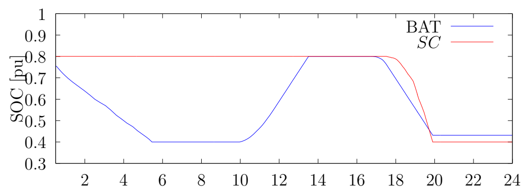

Figure 7: State of charge with winter profile.

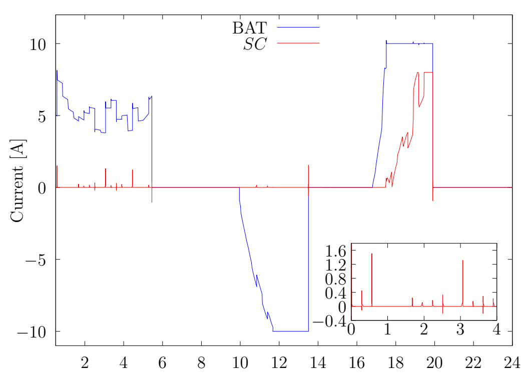

Figure 8: Storage currents with winter profile.

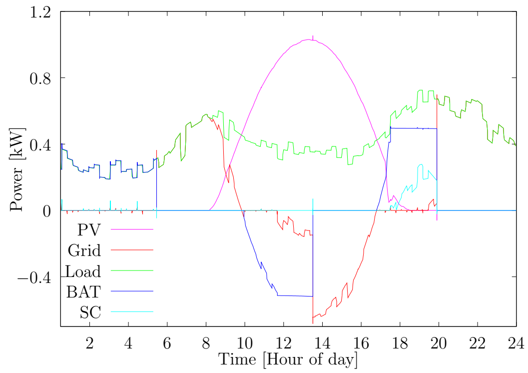

Figure 9: Powers with winter profile.

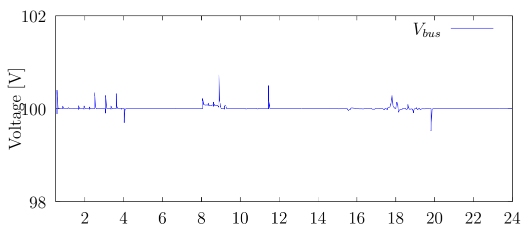

Figure 10: DC bus voltage with summer profile.

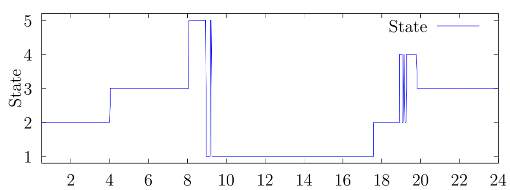

Figure 11: EMS state with summer profile.

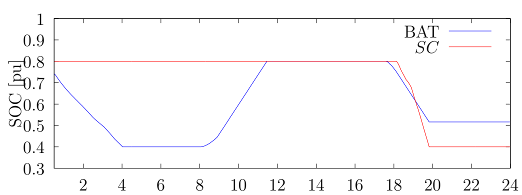

Figure 12: State of charge with summer profile.

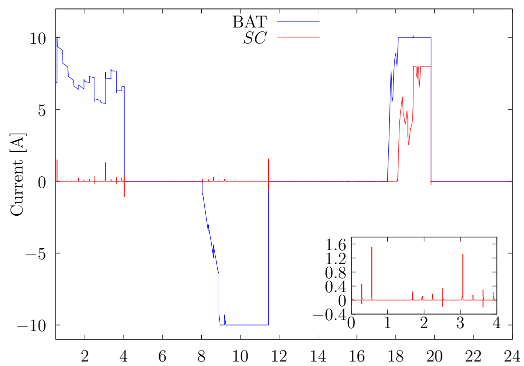

Figure 13: Storage currents with summer profile.

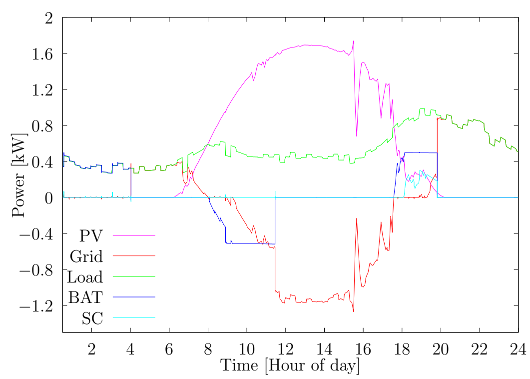

Figure 14: Powers with summer profile.